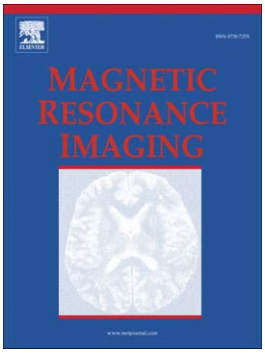

DUSTER: Dynamic contrast enhance up-sampled temporal resolution analysis method

Yoram Louzoun, Moran Artzi, Guy Nadav, James R. Ewing, Dafna Ben Bashat

PII: S0730-725X(15)00309-4
DOI: doi: 10.1016/j.mri.2015.12.014
Reference: MRI 8478

To appear in: *Magnetic Resonance Imaging*

Received date: 6 October 2015
Accepted date: 13 December 2015

Please cite this article as: Louzoun Yoram, Artzi Moran, Nadav Guy, Ewing James R., Bashat Dafna Ben, DUSTER: Dynamic contrast enhance up-sampled temporal resolution analysis method, *Magnetic Resonance Imaging* (2015), doi: 10.1016/j.mri.2015.12.014

DUSTER: Dynamic contrast enhance Up-Sampled Temporal Resolution analysis method

Gilad Liberman[a,b], Yoram Louzoun[c], Moran Artzi[a,d], Guy Nadav[a,e], James R. Ewing[f,g,h]
Dafna Ben Bashat[a,d,i*]

[a]The Functional Brain Center, The Wohl Institute for Advanced Imaging, Tel Aviv Sourasky Medical Center, Tel Aviv; [b]Gonda Multidisciplinary Brain Research Center, Bar-Ilan University, Ramat Gan; [c]Mathematics Department, Bar-Ilan University, Ramat-Gan; [d]Sackler Faculty of Medicine, Tel Aviv University, Tel Aviv; [e]School of Electrical Engineering, Tel Aviv University, Tel Aviv; [f]Department of Neurology, Henry Ford Health System, MI, USA. [g]Department of Physics, Oakland University, MI , USA. [h]Department of Neurology, Wayne State University Medical School, MI, USA. [i]Sagol School of Neuroscience, Tel Aviv University, Tel Aviv; Israel

Funded by: The James S. McDonnell Foundation number 220020176 to D. Ben Bashat.

***Correspondence author:**
Dafna Ben Bashat, Ph.D.
The Functional Brain Center, The Wohl Institute for Advanced Imaging,
Tel Aviv Sourasky Medical Center,
6 Weizmann Street, Tel Aviv, 64239, Israel &
Sackler Faculty of Medicine and Sagol School of Neuroscience
Tel Aviv University,
Haim Levanon St 55, Tel Aviv, Israel
Phone: +972-3-6973953 (o), +972-52-4262515 (m), Fax: +972-3-6973080
E-mail: dafnab@tlvmc.gov.il

ABSTRACT

Dynamic Contrast Enhanced (DCE) MRI using Tofts' model for estimating vascular permeability is widely accepted, yet inter-tissue differences in bolus arrival time (BAT) are generally ignored. In this work we propose a method, incorporating the BAT in the analysis, demonstrating its applicability and advantages in healthy subjects and patients. A method for DCE Up Sampled TEmporal Resolution (DUSTER) analysis is proposed which includes: baseline T_1 map using $DESPOT_1$ analyzed with Flip Angle (FA) correction; preprocessing; raw-signal-to-T_1-to-concentration time curves (CTC) conversion; automatic Arterial Input Function (AIF) extraction at temporal super-resolution; model fitting with model selection while incorporating BAT in the pharmacokinetic (PK) model, and fits contrast agent CTC while using exhaustive search in the BAT dimension in super-resolution. The method was applied to simulated data and to human data from 17 healthy subjects, six patients with glioblastoma, and two patients following stroke. BAT values were compared to time-to-peak (TTP) values extracted from dynamic susceptibility contrast imaging. Results show that the method improved the AIF estimation and allowed extraction of the BAT with a resolution of 0.8sec. In simulations, lower mean relative errors were detected for all PK parameters extracted using DUSTER compared to analysis without BAT correction (v_p:5% vs. 20%, K^{trans}: 9% vs 24% and k^{ep}: 8% vs. 17%, respectively), and BAT estimates demonstrated high correlations (r=0.94, $p<1e^{-10}$) with true values. In real data, high correlations between BAT values were detected when extracted from data acquired with high temporal resolution (2 sec) and sub-sampled standard resolution data (6 sec) (mean r=0.85,$p<1e^{-10}$). BAT and TTP values were significantly correlated in the different brain regions in healthy subjects (mean r=0.72,$p=<1e^{-3}$), as were voxel-wise comparisons in patients (mean r=0.89, $p<1e^{-10}$). In conclusion, incorporating BAT in DCE analysis improves estimation accuracy for the AIF and the PK parameters while providing an additional clinically important parameter.

Keywords: Dynamic Contrast Enhancement, Temporal super resolution, Bolus arrival time, DUSTER

1. Introduction

Dynamic contrast enhanced magnetic resonance imaging (DCE-MRI), also known as permeability imaging, is a noninvasive method that provides clinically important vascular information. In this method, T_1-weighted images (WI) are acquired dynamically during bolus injection of a contrast agent (CA). Several approaches have been suggested to analyze the DCE data, the most widely used of which is a standard kinetic model described by Tofts et al. [1, 2], that was further extended (the Extended Tofts model, ETM). This model is composed of a plasma compartment (with relative volume v_p) and interstitial compartment (relative volume v_e), the forward plasma to interstitium transfer constant K^{trans}, the interstitium to plasma rate constant $k_{ep.}= K^{trans}/ v_e$. All these pharmacokinetic (PK) parameters can be extracted per voxel by deconvolution of the arterial input function (AIF) with the voxel's tissue concentration time curve (CTC). Commonly used methods disregard the inter-tissue differences in bolus arrival time (BAT) that exist between different brain regions, due to either normal or pathological vasculature [3]. These differences are on the order of a few seconds [4], and are usually lower than the temporal resolution commonly used in DCE acquisition (~6sec).

Temporal information regarding the BAT seems to be an important clinical parameter. In clinical settings, the time to peak (TTP) parameter extracted from dynamic susceptibility contrast (DSC) imaging is commonly used for assessment of penumbra in patients following stroke during the acute phase [5] and identification of collateral circulation [6]. DSC is usually acquired using echo-planar imaging (EPI), which enables acquisition of data with high temporal resolution on the order of 1-2 sec, yet with relatively low spatial resolution and with high sensitivity to susceptibility artifacts. In addition, the common analysis does not provide information regarding tissue permeability and neglects its effect, thus resulting in inaccurate estimation of vascular parameters in cases of impaired blood brain barrier (BBB).

Besides the importance of BAT as a physiological parameter, the accuracy of some of the PK parameters (such as the plasma volume v_p) can be significantly affected by the accuracy of the AIF [7, 8]. In common DCE MRI studies, in order to achieve good spatial resolution and coverage, the acquired temporal resolution is about 6 sec; this low temporal resolution often results in inaccurate detection of the amplitude and shape of the AIF [9].

A few studies have used a simple piecewise linear model for fitting the BAT, leaving the AIF in the acquired temporal resolution [10, 11]. In [12], BAT was incorporated in the model, in a

similar manner to the technique used here. However, the BAT estimation accuracy was insufficient for practical use (>1sec inaccuracy). [13] used an analysis in the frequency domain, with implicit robustness to BAT. However, BAT estimates were not produced using this technique.

A functional form for the AIF was suggested in [14]. Automatic blind estimation of the parameters of a similar functional form of the AIF was suggested in [15], which estimated both the AIF and PK parameters in an alternating, iterative manner similar to an Expectation-Maximization (EM) algorithm.

In this study, we propose DUSTER: a DCE Up Sampled TEmporal Resolution method that allows analysis of the data with higher temporal resolution than acquired. This enables a more accurate extraction of the AIF, thus improving the accuracy of the calculated PK parameters and providing an additional parameter, BAT, as part of a kinetic model, in high temporal resolution. The proposed method uses blind estimation of the AIF based on a search in the AIF parameter space, followed by PK modeling utilizing model selection in nested models, similar to that of [16], which has been shown to improve the stability of the estimation. BAT maps with high temporal resolution are presented here for the first time, as an additional hemodynamic parameter.

2. Theory

2.1 Introduction

Converting the MRI signal into concentration time curves (CTCs):

The signal *S* detected with a spoiled gradient echo (SPGR) sequence depends on: the equilibrium longitudinal magnetization of water (M_0) which is related to the proton density; the repetition time (TR); the T_1 value of the tissue; and the flip angle (FA, α) [17]:

$$S = M_0 \cdot \frac{1-\exp\left(-\mathrm{TR}/T_1\right)}{1-\exp\left(-\mathrm{TR}/T_1\right)\cos\left(\alpha\right)}\sin\left(\alpha\right). \quad [1]$$

Other multiplicative factors, which are assumed to remain constant throughout acquisition, such as T_2 and B_0 inhomogeneity effects, can be assumed to be included in M_0. The change in T_2^* due to CA presence is assumed to be negligible due to a small echo-time, although its effects may be visible in cases where the contrast agent concentration is high, such as in arteries.

The T_1 value of a tissue changes in the presence of contrast agent by [1]:

$$R_1(t) = R_{10} + r_1 C(t), \quad [2]$$

where the relaxivity R_1 is the inverse of the relaxation time T_1, R_{10} is the baseline relaxivity of the tissue, r_1 is the relaxivity of the CA and *C(t)* is the concentration of the CA in the tissue at time *t*. Thus, given a signal *S(t)* and the baseline R_{10} value, the CTC (*C(t)*) can be extracted.

Functional form of the AIF: The CTC within the arteries is known as the arterial input function (AIF) ($C_p(t)$). The PK estimation accuracy highly depends on the AIF estimation accuracy. An empirical general functional form for describing the AIF was suggested in [14]. In this study, a slightly different functional form was used in the search for the parameters that best fit a subject's data. As the parameters which control the fine details of the transition from the bolus response into the decay had little variation in our experiments (they are used to maintain the smoothness of the AIF in the boluses-decay junction, and have little variation when used on the smooth data found in patients), we can assume that their values are fixed, without loss of generality. Additionally, the summation was replaced by a (local) maximum operator, which covers a very similar AIF space, but with weaker dependency between the different parameters, an advantage in multiparametric search. Finally, the functional form used in this study was:

$$C_p(t) = \max\left(\alpha_1 G(t-\tau_1,\sigma_1), \alpha_2 G(t-\tau_2,\sigma_2) + \alpha_3 H(t-\tau_3) e^{-\beta(t-\tau 3)}\right). \quad [3]$$

where α_i, τ_i and σ_i are the amplitude, delay and width for the i=1,2 bolus, τ_3 and β are the start time and power for the exponential decay, and $H(\cdot)$ is the Heaviside function.

The kinetic models used: In the Extended Tofts-Kety model [15], the BAT is usually neglected due to the low temporal resolution of the data. Accounting for such a delay in the BAT can be done by a simple shift of the time variable (*t*) within the ETM, resulting in:

$$C(t) = \left(K^{trans} \cdot e^{-k_{ep} \cdot t} + v_p \cdot \delta_t\right) \otimes C_p(t - t_\Delta) \quad [4]$$

where $\otimes$ denotes convolution, K^{trans} is the volume transfer constant between blood plasma and the extracellular, extra-plasma space (EES), and k_{ep} is the rate constant between EES and blood plasma, and t_Δ is the *BAT*, the bolus arrival time value for the specific voxel. The EES volume is denoted v_e and equals K^{trans}/k_{ep}. In the current study, we took into account the BAT in all calculations, allowing the algorithm to search for the PK and BAT parameters in higher temporal resolution than the acquired data.

2.2 AIF Estimation

In our method, the AIF is estimated as the best fit for the data. First, a set of voxels (~30 voxels), which roughly represent the CTC population in the scan, i.e. several voxels from different brain tissues, is automatically chosen by taking representative voxels with various maximal amplitudes and decay rates. The rest of the AIF extraction algorithm is based on this set. We assign a *cost* for any possible AIF by computing the sum (over all the representative CTCs) of the *root-mean-square* errors of fit between the data and the fitted CTC (C(t)), where the fit for a given CTC is calculated using the optimal values of the BAT and PK parameters for this CTC (see next subsection) with the suggested AIF. The estimated AIF is thus the AIF which minimizes this cost. The minimization is done by a full multi-dimensional search in the parameter space of eq. [3] (using MATLAB's fminsearch function, implementing a variation of the Nelder-Mead algorithm [18]). Initial parameters for the search are found by fitting eq. [3] to one of the arterial CTCs (by MATLAB's lsqcurvefit function, implementing the trust-region-reflective algorithm [19, 20]).

2.3 BAT and PK estimation

The PK parameters are estimated for each voxel, given the voxel's CTC and the AIF, using Murase's method [21]. However, we suggest iterating the estimation for a predefined set of time-shifted AIFs; the time-shift value that minimizes the error-of-fit is set to be the BAT value for that voxel. Note that this space can be effectively covered with a reasonable amount of values; in this study we used the range of [-6, 6] seconds at half second intervals.

An error-of-fit that can be significantly decreased by its optimized BAT value suggests high confidence in the estimated BAT value. Contrariwise, an error-of-fit that is almost uniform across different time-shifts indicates low confidence in the BAT estimate. A confidence value for the estimated BAT value was thus set according to the log-likelihood criteria, i.e. one minus the root mean square (RMS) error-of-fit ratio between the BAT value that minimizes the error-of-fit and the second best one, which is at least one second apart.

Similar to [16], model selection was performed by analyzing each voxel's CTC with four nested models, with the BAT parameter added to three of the four following models. Model 0: No visible enhancement. This model consists of zero parameters, and its result is constant - the flat CTC $C(t)=0$. Model 1: No leakage. In normal brain tissue, there is no detectable microvascular leakage of contrast agent. This model has 2 parameters: BAT, v_p. Model 2: Tissue

with CA leakage from the microvasculature, with a negligible re-enter rate. This model has 3 parameters: BAT, v_p and K^{trans}. Model 3: Leakage and re-entrance of the CA, i.e. the full extended Tofts-Kety model with BAT. This model is controlled by 4 parameters: BAT, v_p, K^{trans} and k_{ep}, and v_e can be calculated as K^{trans}/ k_{ep}. AICc are used to choose the best model for each voxel.

3. Materials and methods

3.1 Simulated data

3.1.1 The effects of sampling rate and time shift on the extracted AIF

A realistic AIF was obtained by using the procedures described above on a set of 10 CTCs from manually marked arterial voxels of real data from one subject, and was designated the "true" AIF. The "true" AIF was then sampled with a standard time resolution (every 6 sec) 12 times, each time with a 0.5sec shift, and the parameters characterizing each sampled AIF (eq. [3]) were calculated and compared to that of the "true" AIF.

3.1.2 Accurate extraction of AIF, BAT and PK parameters

Nine simulated three dimensional (3D) data sets, corresponding to data sets obtained from nine patients, were made in order to assess the ability of the method to accurately estimate the AIF, BAT and the other PK parameters in a simulated data with realistic attributes. CTCs were simulated using Eq. [4] for the 9 full VOIs, consisting of 50000-200000 voxels each. The AIF parameters, comprising BAT as well as voxelwise PK parameters used for simulations, were taken from real data of the patients extracted using the proposed method, and perturbed using additive Gaussian noise with standard deviation of 10% of their value. The BAT values were perturbed using the addition of a random delay using the uniform distribution in the [-0.5, 0.5] sec range. The simulated CTCs were sampled at temporal resolution of ~6 seconds, the same temporal resolution at which the original datasets were sampled. An estimation of the noise level per voxel was defined to be the median of the absolute values of the derivative of its CTC. Noise was added to the simulated CTCs using the zero-mean Gaussian distribution with the same standard deviation as their respective original noise estimates, which ranged around SNR=14 in our data. AIFs were estimated for the simulated data and compared to the "true" ones. The BAT and PK parameters extracted using the proposed method, were compared to the PK parameters extracted using the standard method (both using the "true" AIF), i.e. the extended Tofts model

without correcting for BAT, and to the ground truth values – the original parameters used for simulating the data.

3.2 Real data

3.2.1 Subjects

A total of twenty five subjects were included in this study. Seventeen healthy subjects (9 males, mean age 32±10 years old), with no history of neurological disease and without any abnormalities detected on conventional MR images, six patients with biopsy proven glioblastoma (GB), and two patients following acute ischemic stroke, scanned 5 days following the ictus. Inclusion criteria for all subjects were normal glomerular filtration rate and no contraindication to MRI scan. The study was approved by the hospital review board, and written informed consent was obtained from all subjects.

3.2.2 MR protocol

All scans were performed on a 3.0 Tesla MRI scanner (GE Signa EXCITE, Milwaukee, WI, USA) using an eight channel head coil. The DCE data was acquired using multi-phase 3D T_1WI SPGR imaging. Slices were centered around the ventricles for the healthy subjects, and around the tumor/lesion area in patients (defined based on the anatomical images). Multi-phase 3D T1WI SPGR images were acquired before (50 sec), during and after the injection of 0.2 cc/kg contrast agent (Gadolinum DOTAREM), using a power injector, followed by a flush of 20cc saline, both at a constant rate of 5cc/sec. Total scanning time was ~6 min. Other scan parameters were: 12 slices with 5 mm thickness, FOV/matrix = 250mm/256x256, TR/TE = ~5-6/~1.2 msec, FA = 20° with 6 sec temporal resolution unless specified otherwise. For the T_1 maps, variable flip angle SPGR (VFA-SPGR) data was acquired and T_1 maps were calculated based on the driven equilibrium single pulse observation of T_1 (DESPOT1) method [22] using nominal FA values of 30^0,20^0,15^0,10^0,5^0,3^0. DSC was acquired ~10 min after the DCE injection, using a 2D gradient echo (GE) EPI sequence before (15 sec) and during the injection of 0.4 cc/kg contrast agent, using a power injector, followed by a flush of 20cc saline, both at a constant rate of 5cc/sec. Total scanning time was 2 min. Other imaging parameters were: 19 slices, 5 mm thickness with no gap, FOV/matrix= 220-240mm/128x128, slice thickness of 5mm, TR/TE= 1300/30ms and 78-92 repetitions.

3.2.3 Data analysis

DCE analysis was performed using the suggested method: DUSTER, developed in MATLAB. Preprocessing included brain extraction performed using the BET module of the FSL toolbox (http://www.fmrib.ox.ac.uk/fsl) [23], and coregistration of all DCE volumes by rigid transformation using SPM8b's realign module [24]. T_1 values were calculated from VFA-SPGR sequences using the $DESPOT_1$ method [22] with FA correction [25]. The AIF amplitude was normalized by setting the mean v_p in the normal appearing white matter (WM) at one percent. The method used the extended Tofts model including BAT, along with more restricted models and model selection (in a manner similar to [16]).

TTP maps were calculated from the DSC data using the PErfusioN Graphical User INterface (Penguin, http://cfin.au.dk/) software [26] and were compared with the BAT maps.

3.2.4 Validation of the method using high temporal resolution data

Five subjects: two healthy subjects, one patient with glioblastoma (GB, a high-grade tumor), and two patients following stroke, were scanned using DCE with a high temporal resolution of 2 sec. All other acquisition parameters were kept the same as in the data with the standard temporal resolution, however fewer slices were acquired. The data was analyzed twice using the proposed method: first using the complete data with the high resolution sampling rate, and second using a sub-sampling of the data in the time domain, every 6 sec, simulating an analogous conventional scan. A whole brain voxel-wise comparison was performed between the BAT values extracted from the two analyses, in each subject.

3.2.5 Comparison between BAT values and time-to-peak values extracted from dynamic susceptibility contrast imaging

Comparisons between BAT and TTP values (extracted from DSC data) were performed in all subjects (healthy subjects and patients). In healthy subjects, comparison was performed between the mean values of BAT and TTP measure in different brain tissues: white matter (WM), gray matter (GM), arteries and choroid plexus (CP) + veins, obtained following brain segmentation. Segmentation was performed as in [27] on the temporal data (separately for the DCE and DSC data sets in each subject) using k-means algorithm performed in Matlab. In patients, a whole brain voxel-wise comparison was performed between BAT and TTP in each patient.

3.3 Statistical analysis

3.3.1 Simulation data: Mean absolute differences (as percentage of the peak value) were performed between the "true" AIF and the extracted ones. For BAT, mean absolute difference was calculated, and for the PK parameters mean relative absolute differences were calculated, between the true values and the extracted ones.

3.3.2 Real data: The accuracy of the BAT values on the real data acquired with high temporal resolution and the sub-sampled data were tested using correlation analysis on all voxels within the brain where the zero-model was rejected with $p<0.01$, which is to say in those voxels that had sufficient perfusion to demonstrate the presence of CA. In healthy subjects, the correlation between the mean TTP and BAT values within the different brain components were assessed using Pearson's correlation. In addition, a one way ANOVA (SPSS, Chicago, IL, USA), including correction for multiple comparisons was used to compare TTP and BAT values in the different brain components. In patients, the correlation between BAT values and TTP was assessed in each patient voxelwise, on all voxels within the brain where the zero-model in DCE was rejected with $p<0.01$, and where no susceptibility artifacts were visible in DSC.

4. Results

This study proposed DUSTER, a fully automatic analysis method for DCE data and visualization of the results. The software runs on Linux and Windows and has been adapted to accommodate data from GE, Philips and Siemens MRI systems. The analysis pipeline includes baseline T_1 map using DESPOT1 [22] analyzed with the FA correction [25]; motion correction on the 4D data using SPM8b' coregistration module; brain extraction using FSL's brain extraction module; removing and compensation of noisy time-points; raw-signal-to-T_1-to-CTC conversion; B_1 inhomogeneity correction; artery localization; AIF extraction at temporal super- resolution and model fitting with model selection [16]. The software outputs data at all analysis levels (Coregistered raw data, T_1 maps, CTCs, chosen arterial voxels, AIF; model selection, PK and BAT maps, etc.) in an accessible format and a human readable report is produced for each analysis. The user may choose to intervene in a fully manual or semi-automatic way in the voxel selection and in the choice of the AIF. Parameters are available for customization to specific data. The software provides a user-friendly interface for exploration of the results at all levels of the

analysis. DUSTER is designed as an open-source software and is available upon request from the authors.

4.1 Simulated data

4.1.1 The effects of sampling rate and time shift on the extracted AIF

First, we evaluated the error resulting from estimating the AIF using the standard analysis method, i.e. without correcting for BAT. An extracted AIF was marked as the "true" AIF and was sampled with a standard time resolution (every 6 sec) 12 times, each time with a 0.5sec delay (Figure 1). As the sampling time points fall at different positions, the extracted AIF parameters were different. The error in the maximal amplitude of the AIF reached 50%.

4.1.2 Accurate extraction of AIF

Automatic extraction of the AIFs was successfully performed in the nine simulated data sets using the proposed method. The mean correlation between the "true" AIF curves used for the simulation and the extracted ones was mean r value=0.94, $p<1e^{-10}$, and the mean absolute difference over the whole period of the AIF was 5.6%±3.3% (percentage of the peak). Note, that the simulated data was of low temporal resolution (6 sec), yet the proposed method extracted the AIFs in continuous, functional form, while accounting for small delays in the data, and enabled BAT estimation in super-temporal resolution.

4.1.3 BAT and PK parameters estimation

The proposed method enabled extraction of the BAT in all voxels of the 3D simulated data. Extracted BAT values were very similar to the true ones: mean absolute difference of 0.84±0.18sec, with correlation r value=0.92, $p<1e^{-10}$. Notably, the median BAT error was smaller than half a second, and the one second threshold coincided with the 3rd quartile line.

For the parameters directly extracted, i.e. v_p, K^{trans} and k_{ep}, significantly lower absolute relative differences were found using the DUSTER analysis in comparison with the analysis that did not correct for BAT. For v_p: 5.5±1.7% vs. 19.7±6.9%, K^{trans}:9.2±3.2% vs 24.4±8.8% and k_{ep}:8.0±1.6% vs. 16.7±4.3%, respectively, $p<10^{-10}$ for all parameters). Figure 2 shows representative K^{trans} map from simulated data based on a patient with GB, analyzed with and without BAT correction.

4.2 Real data

The method was successfully applied to all datasets acquired with high (2 sec) and standard (6 sec) temporal resolution.

Figure 3 shows an example of the PK; K^{trans}, k_{ep}, v_e, v_p, and BAT maps extracted using DUSTER in a patient with GB. Figure 4 shows an example of a BAT map extracted from standard temporal resolution data in a patient with GB, and examples of time curves obtained from three locations: artery (blue), tumor (green) and choroid plexus (red). As expected, a delay in BAT was detected in the choroid plexus (7.7 sec) compared to the artery. The tumor area showed a delayed BAT of 3.9 sec relative to the artery; this BAT was lower than the acquired temporal resolution, and thus could not be detected using the standard analysis method.

4.2.1 Validation of the method using high temporal resolution data

BAT maps were extracted from the data acquired with high temporal resolution (2 sec), and from the same data sub-sampled to standard temporal resolution (6 sec), in two healthy subjects, two patients with stroke and one patient with GB. Figure 5 shows the BAT maps obtained for the patient with GB, estimated using the proposed method, from the data acquired with high temporal resolution (HTR, b) and from the sub-sampled data (standard temporal resolution STR, c), and the difference between them (d). The proposed analysis method captured the spatial distribution of BAT values in the tumor area. Similar results were obtained in the other subjects. Highly significant whole brain voxel-wise correlations were found in all subjects (n=5) with a mean r value=0.85, $p<1e^{-10}$, with mean median BAT differences of 1.2±0.6 sec.

4.2.2 Comparison with time-to-peak values extracted from DSC imaging

Healthy subjects: mean and standard deviations of relative TTP and BAT values (values are given in arbitrary units relative to the mean value of the entire brain components) in the WM, GM, Arteries and choroid plexus (CP) + veins are given in Table 1. Significant correlation was detected between BAT and TTP parameters for all brain components (r=0.72, $p<0.001$). In addition, multivariate analysis revealed significant differences ($p<0.05$) between GM and arteries, WM and CP+Veins, in both methods. As expected, the bolus arrived first to the arteries and GM, followed by the WM and lastly to the CP + Veins.

Patients: Figure 6 shows examples of BAT and TTP maps in three patients with GB. A high similarity can be seen between maps based on visual inspection, yet while susceptibility artifacts are clearly seen in the TTP maps extracted from DSC, they are not visible in the BAT maps extracted from DCE. Quantitative assessment showed highly significant correlations between BAT and TTP values in all patients based on a whole brain voxel-wise analysis with a mean r value=0.89, $p<1e^{-10}$.

Figure 7 shows an example of BAT maps extracted from high temporal resolution data (b) and from sub-sampled data (c) and TTP maps in a patient following stroke. The proposed method captured the spatial distribution of BAT values in the lesion area similar to that of the TTP which is an important parameter in the assessment of patients following stroke.

Table 1: Comparison with time-to-peak values extracted from dynamic susceptibility contrast imaging in health subjects

Brain component	DSC rTTP (sec)	DCE rBAT (sec)
WM	-0.21±0.56[1]	-0.02±0.77[3]
GM	-0.91±0.48[2]	-0.93±0.74[2]
Arteries	-0.97±0.62[2]	-0.65±0.78[4]
CP + Veins	2.09±0.75[1]	1.60±1.18[1]

rTTP, rBAT = values relative to the mean value of the entire brain components. Significantly different ($p<0.05$, Corrected for multiple comparisons) from: 1all other components, 2WM and CP + Veins, 3GM and CP + Veins, 4CP + Veins.

5. Discussion

This study proposed DUSTER, a fully automatic analysis method for DCE data with visualization of the results. DUSTER is an open-source software that is available upon request from the authors. DUSTER is based on the Extended Tofts Model, includes FA correction for the T_1 mapping, accounting for differences in the BAT by incorporating BAT in the PK model and fitting the contrast agent concentration time curves while using exhaustive search in the BAT dimension in super-resolution, and includes model selection. Results show that the method improves the AIF and PK parameters estimation and allows extraction of the BAT parameter with a resolution of 0.8sec. High correlations were detected between BAT and TTP values in the different brain regions in healthy subjects and in voxel-wise comparisons in patients.

Accounting for time-shifts during the blind estimation of the AIF, rather than assuming uniform delay over the chosen voxels can improve the estimation of the AIF in terms of overall shape and mainly the first bolus parameters (amplitude and width). While the transfer constants K^{trans} and k_{ep}, which are affected by the slow behavior of the system, are not expected to be

strongly influenced by such change, improvement in AIF estimation accuracy affects the parameters directly related to the first bolus - v_p and BAT. In addition, taking the BAT into account is expected to improve flow estimation under an extended model.

DCE-extracted BAT maps are presented here for the first time. The BAT parameter extracted using DUSTER provides an additional PK parameter. This parameter can differentiate between brain components in healthy tissue supporting the tissue vascularity. Results are in accordance with previously reported studies on the temporal differences between brain components [28, 29]. In addition, this parameter showed a delay in tumor areas in patients with GB and in lesion area in patients following stroke, similar to the TTP parameter. TTP is an important parameter in stroke imaging for the assessment of penumbra during the acute phase [5]. The high correlation between BAT and TTP suggests the usefulness of DCE in the assessment of patients following stroke. While DSC is easily acquired with high temporal resolution, it suffers from low spatial resolution, image distortions and high sensitivity to susceptibility artifacts.

DSC data is usually acquired with a higher temporal resolution of about 1-2 sec, and therefore temporal parameters such as Start Time and TTP can be estimated. The calculated TTP parameter takes into account the contrast agent dispersion (resulting from blood flow). This parameter is neglected in the current DCE analysis. Thus, discrepancy between the TTP and BAT maps can stem from the dispersion of the bolus in the vasculature between the feeding artery and the tissue's voxel. Including CBF in the DCE model is thus recommended and can improve the accuracy of calculated PK and BAT parameters. Yet, it requires true acquisition of high-temporal data (11). The temporal resolution of DCE acquisition is usually on the order of a few seconds and is limited by the spatial resolution and brain coverage required for clinical use, resulting in inaccurate CBF estimation. With the introduction of new MR systems and software, this limitation may become less relevant.

This study focused on Tofts model and its derivatives. Possible sources of error include flow effects [30] and water exchange effects [31, 32]. In order to extract flow accurately, data with higher temporal resolution is required. Neglecting this parameter in the model may cause overestimation of the permeability. Neglecting the water exchange may cause underestimation of the plasma volume, yet in the large flip angle range commonly used in DCE (20°-30°), this is not expected to be a major effect.

6. Conclusion

This study proposes the DUSTER (DCE Up-Sampled TEmporal Resolution) analysis method, which allows extraction of an additional parameter, BAT, relating to the tissue's vasculature, in an up sampled temporal resolution. The proposed method resulted in a better estimation of the AIF and the extracted PK parameters. The BAT may have clinical importance in the diagnosis of patients with vascular diseases and in therapy response assessment.

Figure captions

Figure 1: The effect of sampling rate and time shift on the extracted arterial input function (AIF). True AIF and the curves resulting from sampling of 6 seconds, where the start point is shifted by 0 to 5.5 seconds, in half second intervals. The inset focuses around the peak.

Figure 2: Representative *K*trans map from simulated data based on a patient with GB, analyzed with and without BAT correction. (a) Ktrans map used for the simulation (b) Estimated Ktrans maps, with and without BAT correction, and the absolute differences maps.

Figure 3: An example of the PK and BAT maps extracted using DUSTER from a patient with GB. (a) T1W post contrast agent image (T1W+CA), (b) Ktrans maps, in min-1 [0.01, 0.3] (c) kep maps, in min-1 [0, 1] (d) ve maps, in arbitrary units (a.u.) (relative volume) [0, 0.3], (e) vp maps, in a.u. (relative volume) [0, 0.01], (f) BAT maps, in seconds [-6, 6].

Figure 4: Data obtained from a patient with GB, and time curves obtained from three locations: artery (blue), tumor (green) and CP (red). (a) T1W post contrast agent image (T1W+CA), (b) BAT map, (c) CTCs, (d) CTCs with normalized scale zoomed to the first minute to visually emphasize BAT difference.

Figure 5: Comparison of BAT maps extracted from high-temporal-resolution (HTR) and sub-sampled data to standard temporal resolution (STR) in a patient with GB. (a) T1W post contrast agent image (T1W+CA), (b) BAT map obtained from HTR data (c) BAT map obtained from the data sub-sampled STR data (d) BAT differences map.

Figure 6: Comparisons between BAT and TTP maps obtained from three patients with GB. (a) T1W post contrast agent images (T1W+CA); (b) BAT maps extracted from DCE (with standard temporal resolution - STR of 6 sec); and (c) TTP maps extracted from DSC.

Figure 7: Comparison between BAT and TTP maps obtained from a patient with acute ischemic stroke. (a) Diffusion weighted image (DWI) showing the ischemic lesion area; (b) high temporal resolution (HTR, 2sec) BAT map (d) down sampled standard temporal resolution (STR, 6sec) BAT map; and (c) TTP map.

Acknowledgments

To Vicki Myers for editorial assistance

References

1. Tofts PS, Brix G, Buckley DL, Evelhoch JL, Henderson E, Knopp MV, Larsson HB, Lee T-Y, Mayr NA, Parker GJ (1999) Estimating kinetic parameters from dynamic contrast-enhanced T 1-weighted MRI of a diffusable tracer: standardized quantities and symbols. Journal of Magnetic Resonance Imaging 10: 223-232
2. Tofts PS, Kermode AG (1991) Measurement of the blood-brain barrier permeability and leakage space using dynamic MR imaging. 1. Fundamental concepts. Magnetic Resonance in Medicine 17: 357-367
3. Kao YH, Teng MMH, Liu KC, Lam IP, Lin YC (2008) Hemodynamic segmentation of MR perfusion images in patients with unilateral carotid stenosis using independent component analysis. Journal of Magnetic Resonance Imaging 28: 1125-1132
4. Artzi M, Aizenstein O, Abramovitch R, Bashat DB (2013) MRI multiparametric hemodynamic characterization of the normal brain. Neuroscience 240: 269-276 doi:10.1016/j.neuroscience.2013.03.004 S0306-4522(13)00219-4 [pii]
5. Muir KW, Santosh C (2005) Imaging of acute stroke and transient ischaemic attack. J Neurol Neurosurg Psychiatry 76 Suppl 3: iii19-iii28 doi:76/suppl_3/iii19 [pii] 10.1136/jnnp.2005.075168
6. Hermier M, Ibrahim AS, Wiart M, Adeleine P, Cotton F, Dardel P, Derex L, Berthezene Y, Nighoghossian N, Froment JC (2003) The delayed perfusion sign at MRI. J Neuroradiol 30: 172-179 doi:MDOI-JNR-06-2003-30-3-0150-9861-101019-ART05 [pii]
7. Chen JJ, Smith MR, Frayne R (2005) The impact of partial-volume effects in dynamic susceptibility contrast magnetic resonance perfusion imaging. Journal of Magnetic Resonance Imaging 22: 390-399
8. Wendland MF, Saeed M, Yu KK, Roberts TP, Lauerma K, Derugin N, Varadarajan J, Watson AD, Higgins CB (1994) Inversion recovery EPI of bolus transit in rat myocardium using intravascular and extravascular gadolinium-based MR contrast media: Dose effects on peak signal enhancement. Magnetic Resonance in Medicine 32: 319-329
9. Henderson E, Rutt BK, Lee T-Y (1998) Temporal sampling requirements for the tracer kinetics modeling of breast disease. Magnetic resonance imaging 16: 1057-1073

10. Kim J, Leira EC, Callison RC, Ludwig B, Moritani T, Magnotta VA, Madsen MT (2010) Toward fully automated processing of dynamic susceptibility contrast perfusion MRI for acute ischemic cerebral stroke. Computer methods and programs in biomedicine 98: 204-213
11. Singh A, Rathore RKS, Haris M, Verma SK, Husain N, Gupta RK (2009) Improved bolus arrival time and arterial input function estimation for tracer kinetic analysis in DCE-MRI. Journal of Magnetic Resonance Imaging 29: 166-176
12. Kershaw LE, Buckley DL (2006) Precision in measurements of perfusion and microvascular permeability with T1-weighted dynamic contrast-enhanced MRI. Magnetic Resonance in Medicine 56: 986-992
13. Orton MR, Collins DJ, Walker-Samuel S, d'Arcy JA, Hawkes DJ, Atkinson D, Leach MO (2007) Bayesian estimation of pharmacokinetic parameters for DCE-MRI with a robust treatment of enhancement onset time. Physics in medicine and biology 52: 2393
14. Parker GJ, Roberts C, Macdonald A, Buonaccorsi GA, Cheung S, Buckley DL, Jackson A, Watson Y, Davies K, Jayson GC (2006) Experimentally-derived functional form for a population-averaged high-temporal-resolution arterial input function for dynamic contrast-enhanced MRI. Magnetic Resonance in Medicine 56: 993-1000
15. Fluckiger JU, Schabel MC, DiBella EV (2009) Model-based blind estimation of kinetic parameters in dynamic contrast enhanced (DCE)-MRI. Magnetic Resonance in Medicine 62: 1477-1486
16. Bagher-Ebadian H, Jain R, Nejad-Davarani SP, Mikkelsen T, Lu M, Jiang Q, Scarpace L, Arbab AS, Narang J, Soltanian-Zadeh H, Paudyal R, Ewing JR (2011) Model selection for DCE-T1 studies in glioblastoma. Magnetic Resonance in Medicine
17. Deoni SC (2007) High-resolution T1 mapping of the brain at 3T with driven equilibrium single pulse observation of T1 with high-speed incorporation of RF field inhomogeneities (DESPOT1-HIFI). Journal of Magnetic Resonance Imaging 26: 1106-1111
18. Lagarias JC, Reeds JA, Wright MH, Wright PE (1998) Convergence Properties of the Nelder--Mead Simplex Method in Low Dimensions. SIAM journal on optimization 9: 112-147
19. Coleman TF, Li Y (1994) On the convergence of interior-reflective Newton methods for nonlinear minimization subject to bounds. Mathematical programming 67: 189-224

20. Coleman TF, Li Y (1996) An interior trust region approach for nonlinear minimization subject to bounds. SIAM journal on optimization 6: 418-445
21. Murase K (2004) Efficient method for calculating kinetic parameters using T1-weighted dynamic contrast-enhanced magnetic resonance imaging. Magn Reson Med 51: 858-862 doi:10.1002/mrm.20022
22. Deoni SC, Peters TM, Rutt BK (2005) High-resolution T1 and T2 mapping of the brain in a clinically acceptable time with DESPOT1 and DESPOT2. Magnetic Resonance in Medicine 53: 237-241
23. Smith SM (2002) Fast robust automated brain extraction. Hum Brain Map 17: 143-155
24. Wells WMI, Viola P, Atsumi H, Nakajima S, Kikinis R (1996) Multi-modal volume registration by maximization of mutual information. Med Imag Anal 1: 35 - 51
25. Liberman G, Louzoun Y, Ben Bashat D (2013) T1 Mapping using variable flip angle SPGR data with flip angle correction. Journal of Magnetic Resonance Imaging
26. Østergaard L, Weisskoff RM, Chesler DA, Gyldensted C, Rosen BR (1996) High resolution measurement of cerebral blood flow using intravascular tracer bolus passages. Part I: Mathematical approach and statistical analysis. Magnetic Resonance in Medicine 36: 715-725
27. Artzi M, Guy N, Liberman G, Aizenstein O, Ben Bashat D (2014) Brain blood volume assessment using DCE in comparison to DSC methods. The International Society for Magnetic Resonance in Medicine. Milan, Italy
28. Artzi M, Aizenstein O, Hendler T, Ben Bashat D (2011) Unsupervised multiparametric classification of dynamic susceptibility contrast imaging: study of the healthy brain. Neuroimage 56: 858-864 doi:S1053-8119(11)00303-X [pii] 10.1016/j.neuroimage.2011.03.027
29. Kao YH, Guo WY, Wu YT, Liu KC, Chai WY, Lin CY, Hwang YS, Jy-Kang Liou A, Wu HM, Cheng HC, Yeh TC, Hsieh JC, Mu Huo Teng M (2003) Hemodynamic segmentation of MR brain perfusion images using independent component analysis, thresholding, and Bayesian estimation. Magn Reson Med 49: 885-894 doi:10.1002/mrm.10440
30. Nadav G, Liberman G, Artzi M, Kiryati N, Ben Bashat D (2014) Flow and permeability estimation from DCE data: Comparison of 2-compartment exchange and Tofts models Proc Intl Soc Mag Reson Med

31. Paudyal R, Bagher-Ebadian H, Nagaraja TN, Fenstermacher JD, Ewing J (2011) Modeling of Look-Locker estimates of the magnetic resonance imaging estimate of longitudinal relaxation rate in tissue after contrast administration. Magnetic Resonance in Medicine 66: 1432-1444
32. Ewing JR, Bagher-Ebadian H (2013) Model selection in measures of vascular parameters using dynamic contrast-enhanced MRI: experimental and clinical applications. NMR in Biomedicine 26: 1028-1041

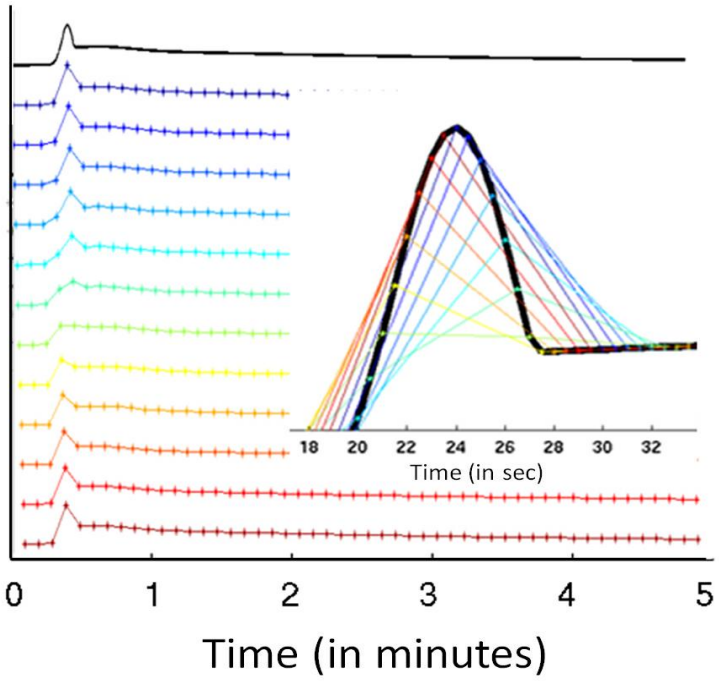

Figure 1

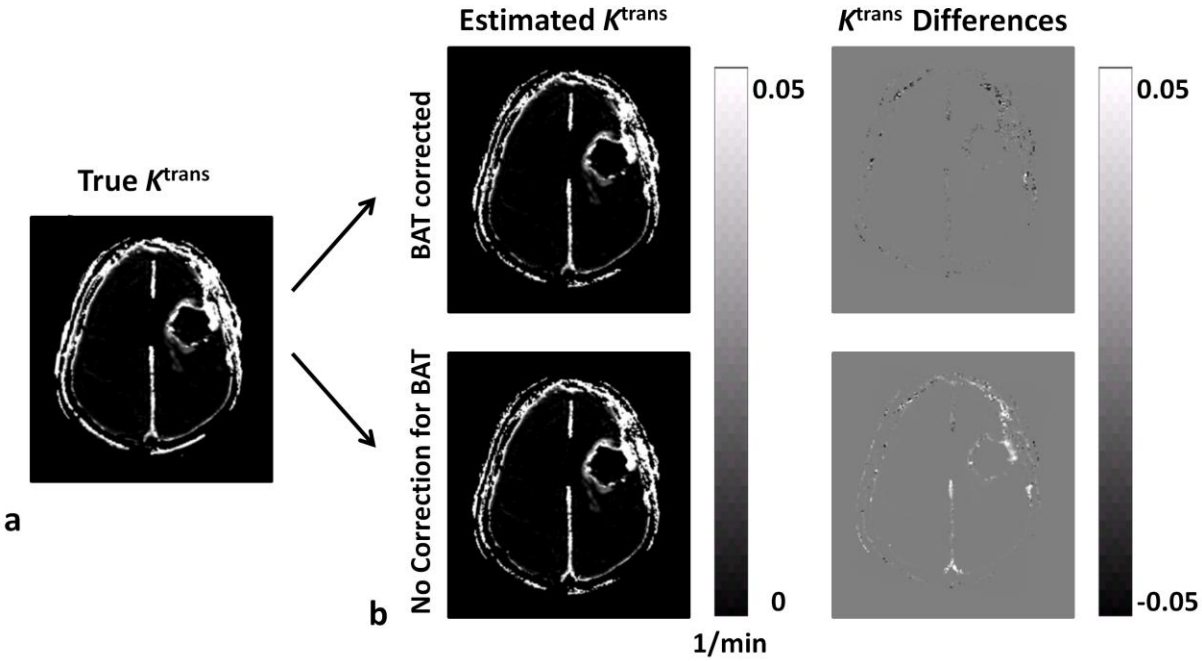

Figure 2

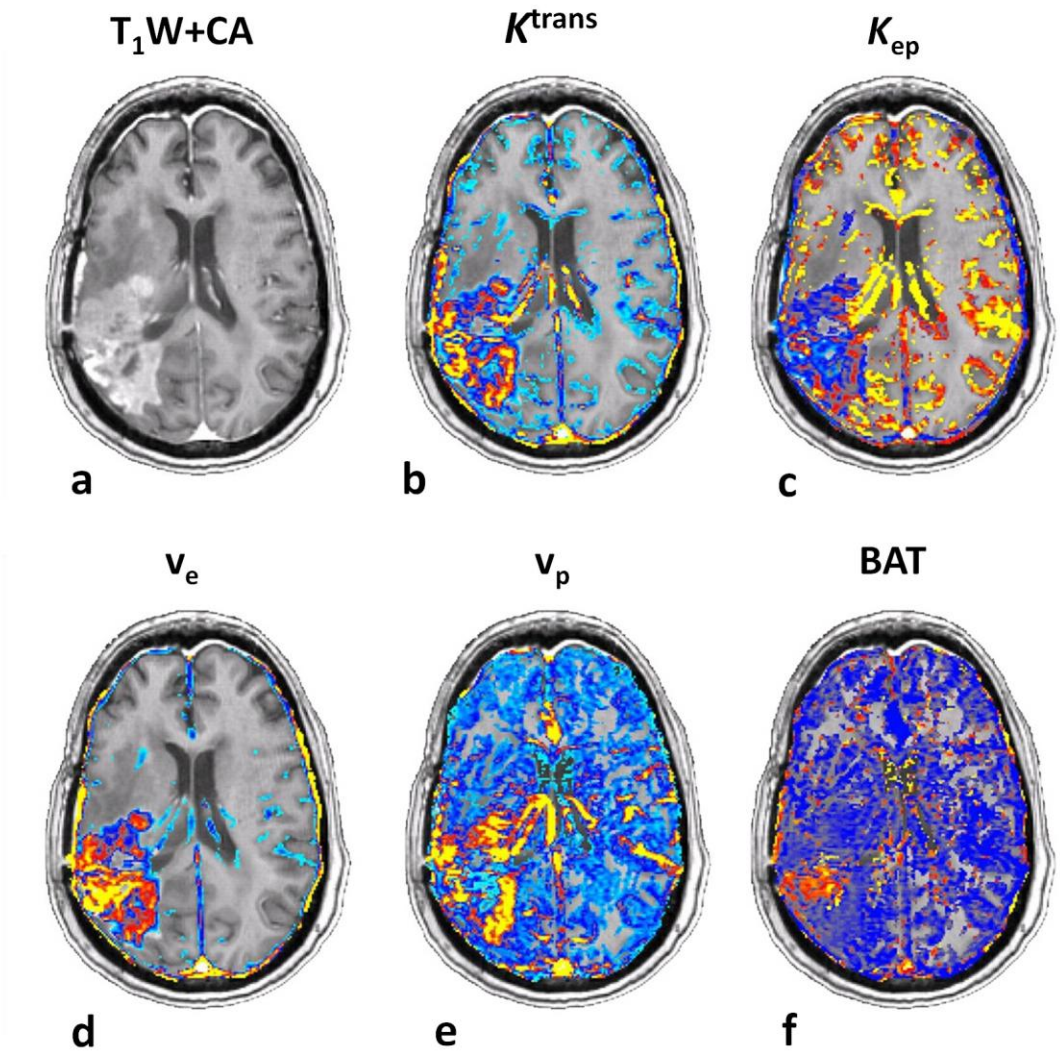

Figure 3

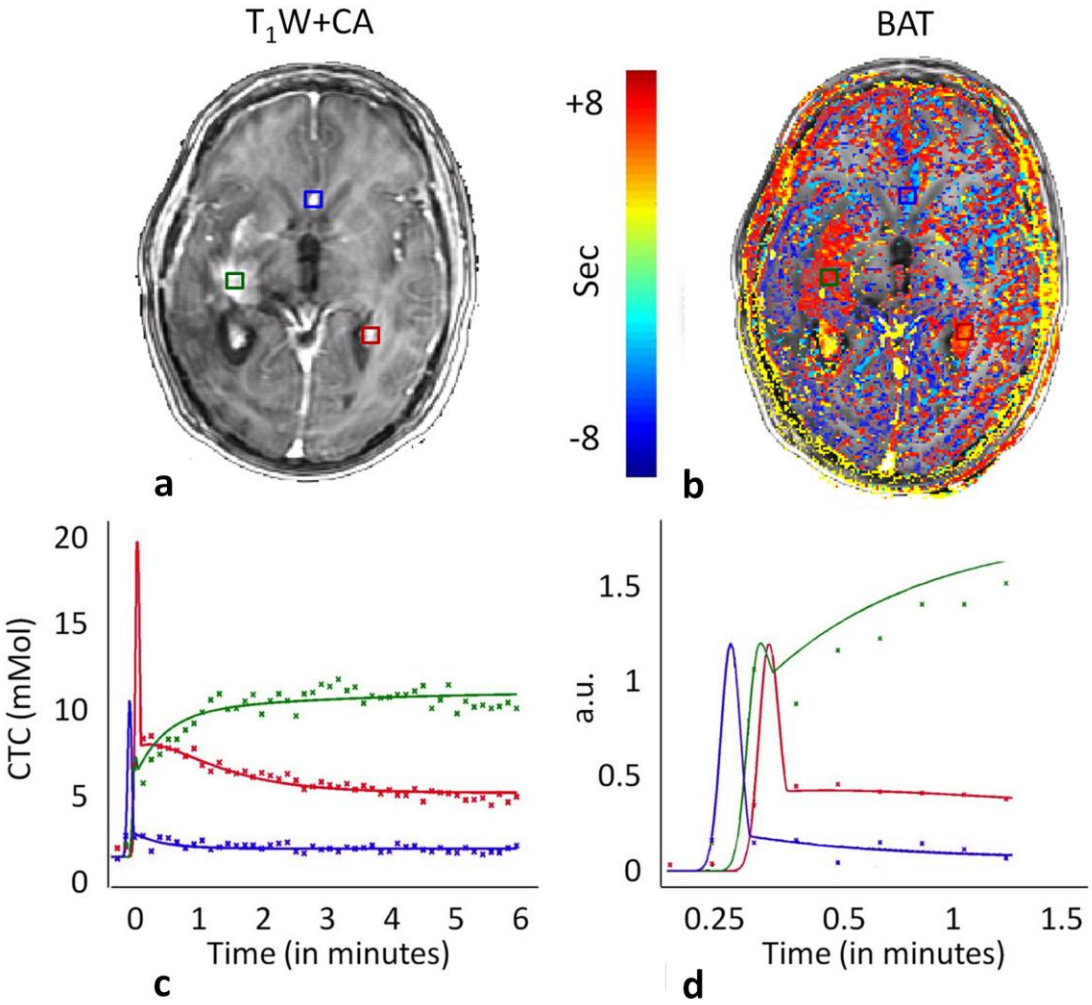

Figure 4

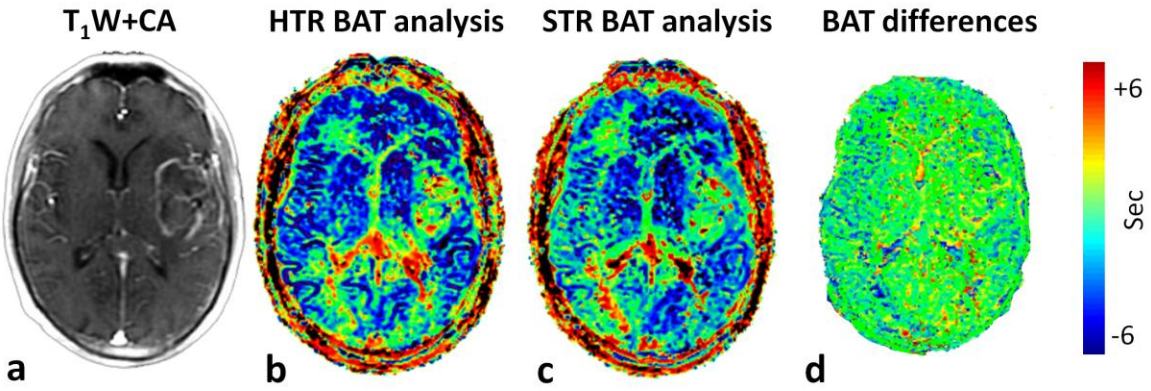

Figure 5

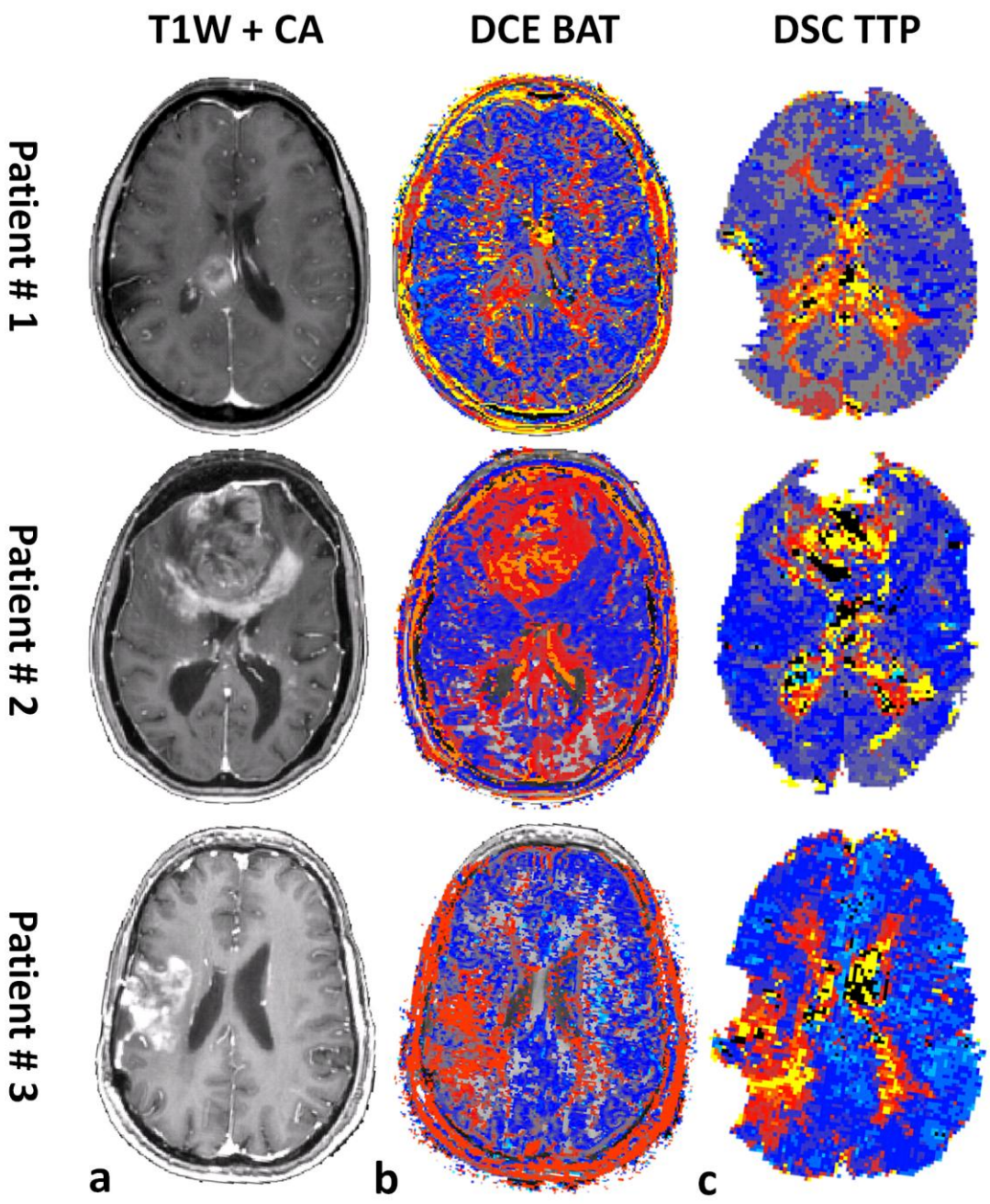

Figure 6

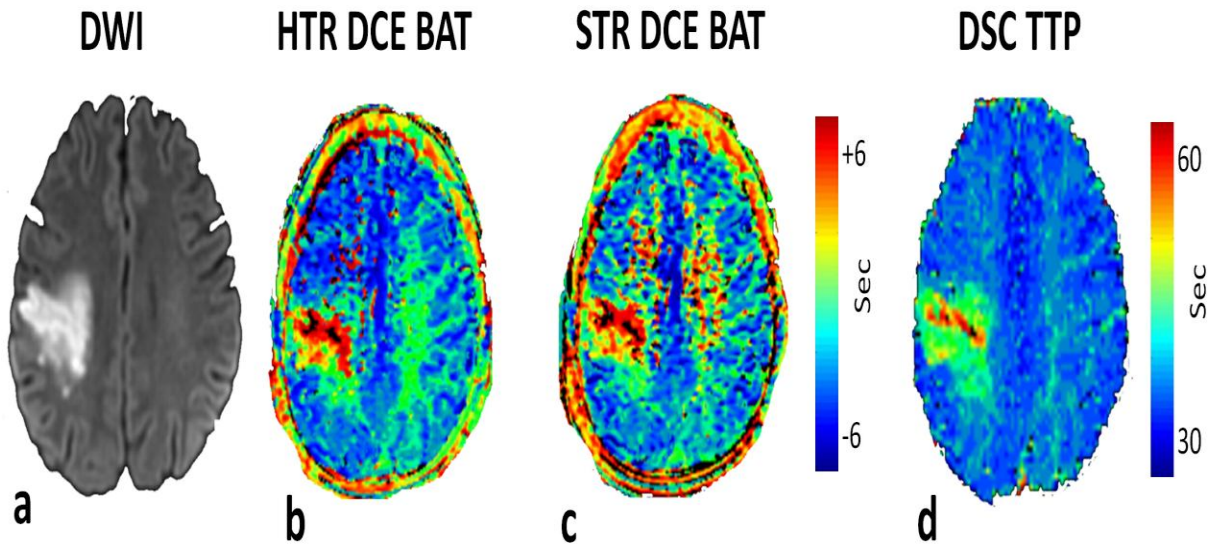

Figure 7